Characterization of the Nanoscale in Triacylglycerol Crystal Networks

ARTICLE *in* CRYSTAL GROWTH & DESIGN · JULY 2010

Impact Factor: 4.89 · DOI: 10.1021/cg100468e

2 AUTHORS:

Nuria Acevedo
Iowa State University
24 PUBLICATIONS **305** CITATIONS
SEE PROFILE

Alejandro Gregorio Marangoni
University of Guelph
342 PUBLICATIONS **6,862** CITATIONS
SEE PROFILE

DOI: 10.1021/cg100468e

CRYSTAL GROWTH & DESIGN Article

2010, Vol. 10
3327–3333

Characterization of the Nanoscale in Triacylglycerol Crystal Networks

Nuria C. Acevedo and Alejandro G. Marangoni*

Guelph-Waterloo Physics Institute, Centre for Food & Soft Materials Science, Department of Food Science, University of Guelph, 50 Stone Road East, Guelph, Ontario, Canada, N1G 2W1

Received April 8, 2010; Revised Manuscript Received June 11, 2010

ABSTRACT: Here we report on the characterization of the nanoscale in triacylglycerol crystal networks of edible fats. Blends of tristearin and triolein were prepared in proportions between 20 and 100% w/w to achieve a wide range of supersaturations. Crystal networks were subjected to mechanical disruption using isobutanol at 10 °C and visualized using cryogenic transmission electron microscopy (cryo-TEM). This method allowed the breakdown of spherulitic structures into their primary crystals: nanoplatelets of approximate sizes 150 × 60 × 30 nm to 370 × 160 × 40 nm depending on supersaturation conditions, and a length to width aspect ratio of 2.3. The method also allowed the visualization of bimolecular triacylglycerol lamellae within a cross-section of a nanoplatelet. The tristearin *d*-spacing (~4.5 nm) and domain size (30−50 nm) of the (001) plane, by cryo-TEM and small-angle X-ray diffraction, agreed quantitatively. Scherrer analysis provided an accurate estimate of the cross-sectional thickness of the nanoplatelets and was linearly related to the length and width of the corresponding nanoplatelets, allowing in principle the use of small-angle X-ray diffraction as a rapid and accurate "nanocrystal sizer". A pictorial representation of the hierarchical structure of a triacylglycerol crystal network is presented. This work opens up the possibility of nanomanipulation of the structure of fats to target specific physical properties and physiological response.

Introduction

Edible fats are a special class of plastic polycrystalline aliphatic soft matter. The structure of such materials is hierarchical and complex.[1−3] Triacylglycerol (TAG) molecules crystallize from the melt to form crystals which then aggregate via mass and heat transfer limited aggregation processes to form higher structural levels until a space filling network is formed. Liquid oil can be very efficiently trapped within this network to very high volume fractions, thus enhancing the plastic rheological properties. Thus, fat can be considered a classic polycrystalline material resembling waxes, but it can also be considered a colloidal gel/crystal due to the formation of an oleogel crystal network. The beauty of these materials is that they can behave as either, and attempts at predicting their macroscopic functionality can be based on either approach. For example, good quality chocolate needs to be crystallized and stabilized in a particular triclinic form commonly called the form V.[4] This form has been associated with desirable melting behavior and characteristic mechanical properties. On the other hand, good quality butter or margarine will contain ~30% volume fraction of liquid oil and needs to be structured by small crystallites < 10 μm in size. This oleogel will then possess the correct extensional flow properties for plastic deformation, that is, spreadability, and mouthfeel.

The importance of the structure of this fat crystal network has been recognized for close to 50 years.[1,3,5−15] The growth of a TAG crystal network starts when the TAG molecules present in the sample arrange and crystallize from the melt into "primary crystals". Once the "primary crystals" are formed, they aggregate via a mass- and heat-transfer limited process to form polycrystals and crystal aggregates at the microstructural scale. The aggregation process continues until a three-dimensional network is created.

Many microscopy techniques have been used in the study of fat crystal morphology. Polarized light microscopy (PLM) has provided essential qualitative and quantitative information on the microstructural characterization of fats. It can distinguish between solid and liquid phases since fat crystals are birefringent and appear bright under polarized light, whereas liquid fat remains dark.[16−18] This technique has a lower limit of resolution of about 1−2 μm. Cryogenic scanning electron microscopy (cryo-SEM) allows for the study of surface topography[9,17] but is inherently a low resolution technique (~5 μm) since the contrast between fat crystals and "frozen" oil is poor. Confocal scanning light microscopy (CSLM) and multiple photon microscopy (MFM) complement both conventional light microscopy and electron microscopy, allowing the observation of structure in thick samples at greater depths (60−200 μm); however, the resolution attainable is relatively low (~3−5 μm) and both require the incorporation of a fluorescent dye in the sample.[19,20] Three-dimensional polarized light microscopy coupled to wide-field deconvolution has been successfully used to visualize low-solids' content fat crystal network structure in 300 μm thick samples.[21] However, a lower limit of resolution of 2−5 μm could not be improved. Transmission electron microscopy (TEM) enables a much higher resolution and has been employed for the observation of TAG crystals obtained by crystallization from an aqueous emulsion of TAGs dissolved in an organic solvent.[22,23] As far as we know, only one study could be found on the visualization and quantification of native fat crystal microstructure using TEM.[24]

One of the major problems associated with the microscopic observation of fat structure is that appropriate analysis is hampered by the presence of oil between the crystals. Surprisingly, only very few studies have been focused on the removal of liquid oil from the solid fat crystal network. In contrast, the characterization of xerogels derived from organogels is a well-developed area of endeavor.[25] Liquid oil has

*Corresponding author. Telephone: +1-519-824-4120 x54340. Fax: +1-519-824-6631. E-mail: amarango@uoguelph.ca.

Published on Web 07/08/2010

Table 1. Melting Temperatures (T_m), Enthalpies of Melting (ΔH_m), Chemical Potential Difference ($\Delta\mu$), and Supersaturation Values ($\ln\beta$) for Blends of Fully Hydrogenated Canola Oil (FHCO) and High Oleic Sunflower Oil (HOSO) in the β Polymorphic Form

% S^a	20	30	40	50	60	70	80	90	100
ΔH_m (kJ mol^{-1})^b	32.5	61.4	73.4	95.4	106.8	120.3	129.6	148.4	164.9
T_m (K)^c	333.3	336.5	337.4	338.8	340.7	342.0	344.2	344.4	344.9
$\Delta\mu$ (kJ mol^{-1})^d	10.06	11.52	11.93	12.55	13.41	13.98	14.94	15.05	15.25
$\ln\beta^d$	3.9	4.4	4.6	4.8	5.1	5.4	5.7	5.8	5.9

[a] % of hardstock. [b] Considering tristearin MW = 891.48 g mol^{-1}, %SD < 2.5%. [c] %SD < 0.5%. [d] %SD < 0.1%.

been removed using cold organic solvents or aqueous detergent solutions, thus providing important insights into the structure of the solid TAG network.[9,16,24,26,27] Although some studies have been successful in terms of the qualitative observation of single fat crystals and some quantification of their dimensions,[24,26,27] systematic studies on the nanostructure of fat crystal networks still remain to be performed. Moreover, the realization of the existence of a TAG crystal nanoscale and its relationship to higher levels of structure cannot be found in the literature. It was evident that special preparation techniques are required to achieve an appropriate nanocrystal extraction, isolation, observation, and characterization.

Powder X-ray diffraction (XRD) is one of the best methods to study the solid state of TAGs. The usual information reported are the long and short spacing of crystals which define a particular polymorphic form, yet X-ray diffraction patterns can also provide additional and valuable information on the structure of a fat crystal network. The Scherrer model can be used to characterize the crystalline domain size: a characteristic dimension of the primary crystals[28] through the use of the width at half the maximum intensity of a specific diffraction peak, the (001) plane reflection in TAGs. This analysis could potentially prove to be very useful in the characterization of fat crystalline nanostructure.

The purpose of this work was to carry out a qualitative and quantitative systematic study of the nanostructure in fat blends of fully hydrogenated canola oil (FHCO) and high oleic sunflower oil (HOSO). We expect our findings to be the initial steps in the development of a qualitative and quantitative understanding of the relationship between the nanostructure (never considered before) and the macroscopic properties in fat crystal networks.

Experimental Section

Materials. Fully hydrogenated canola oil (FHCO) and high oleic sunflower oil (HOSO) were generously provided by Bunge Canada (Toronto, Canada) and Nealanders (Toronto, Canada), respectively. All chemicals and organic solvents were purchased from Fisher Scientific and Sigma-Aldrich (ON, Canada). Ahmadi et al.[29] reported the fatty acid composition of FHCO and HOSO. FHCO contained ~88% stearic acid (18:0), ~9% of palmitic acid (16:0), and ~2% arachidic acid (20:0). The predominant fatty acids in HOSO were oleic acid (18:1), ~77%, while only small amounts of linoleic acid (18:2), stearic acid, and palmitic acid were present, ~8%, ~6%, and~5%, respectively.

Blend Preparation. Blends of FHCO and HOSO were mixed in 10% increments (w/w) ranging from 20% to 100% of hardstock. The blends were held at 80 °C for 30 min to erase crystal memory. Then, the samples were stored at a temperature 40 °C higher than the corresponding melting temperature (T_m) of the particular blend (Table 1) in order to promote the β polymorphic (triclinic) form. X-ray diffraction patterns were collected at 20 °C to confirm the presence of the signals corresponding to the desired polymorphic form. Subsequently, blends were kept at 20 °C prior to analysis.

Differential Scanning Calorimetry (DSC). A differential scanning calorimeter (DSC; Q1000, TA Instruments, Mississauga, ON, Canada) was used in the thermal analysis of the different fat blends. The instrument heat capacity response was calibrated with sapphire, and the heat flow was calibrated with indium. Approximately 10 mg of the fat sample was placed in alodined pans and sealed hermetically (an empty pan served as reference). All measurements were performed at a heating rate of 5 °C/min. Thermograms were evaluated using TA Instruments Universal Analysis Software. The peak melting temperature (T_m) and the enthalpy of melting (ΔH_m) were determined. The average and standard deviation of four replicates are reported in this study.

Polarized Light Microscopy. Polarized light microscopy (PLM) was used to observe fat microstructure. A small drop of preheated fat blend (80 °C) was placed on a preheated slide at the same temperature, and a coverslip was then gently laid over the fat drop to remove air and spread the fat. Slides were stored at conditions at which the β-crystal polymorphic form was favored. The slide was then transferred into a thermostatically controlled microscope stage at 20 °C (model LTS 350, Linkam Scientific Instruments, Surrey, UK). Samples were imaged using a Leica DM RXA2 microscope with polarized light (Leica Microsystems, Richmond Hill, Canada) and equipped with a CCD camera (Q Imaging Retiga 1300, Burnaby, BC, Canada). All images were acquired using a 50× objective lens (Leica, Germany). The camera was set for autoexposure. Openlab 5.5.0 software (Improvision, Waltham, MA, USA) was used to acquire images. Focused images were stored as uncompressed 8-bit (256 grays) grayscale TIFF files with a 1280 × 1.024 spatial resolution. Five images were captured from each of five specimens prepared.

Microstructural analysis was carried out by image analysis employing the Adobe Photoshop 5.5 software (Adobe Systems Inc., San Jose, California, USA) and filters from the Fovea Pro 4.0 software (Reindeer Graphics, Inc., Asheville, NC, USA). A manual thresholding was applied to all the pictures to convert the grayscale images to binary images, in order to discriminate between features and background and to measure the features sizes. The microstructural elements were determined using the filter tools included in the Fovea Pro software.

Powder XRD Analysis. XRD data were collected using a Rigaku Multiflex Powder X-ray diffractometer (Rigakug, Japan). The copper lamp (λ = 1.54 Å for copper) was set to 40 kV and 44 mA. A 0.57 divergence slit, 0.57 scatter slit, and 0.3 mm receiving slit were used. For the small-angle X-ray diffraction analysis (SAXD) the samples were scanned from 0.9 to 8 deg at 0.02°/min. The wide-angle X-ray diffraction analysis (WAXD) was carried out scanning the samples from 16 to 35 deg at 0.5°/min. PeakFit software (Seasolve, Framingham, MA, USA) was used to analyze the obtained patterns in both SAXD and WAXD.

From the SAXD patterns, the crystalline domain size (ξ) can be calculated by the well-known Scherrer formula which is limited to nanoscale particles, and it is not applicable to sizes larger than about 100 nm:[28]

$$\xi = \frac{K\lambda}{\text{fwhm}\cos(\theta)} \quad (1)$$

where K is the shape factor, θ is the diffraction angle, fwhm is the full width at half of the maximum peak height in radians (usually from the first small angle reflection corresponding to the (001) plane), and λ is the wavelength of the X-ray. The dimensionless shape factor provides information about the "roundness" of the particle. For a spherical particle, the shape factor is 1, and for all other particles it is smaller than 1. A value of 0.9 is usually used for crystallites of unknown shape and is the value used in this study.

Cryogenic Transmission Electron Microscopy (Cryo-TEM). In order to discard the oil fraction and favor single crystals observation, fat blends were treated at 10 °C as follows. Fat samples were

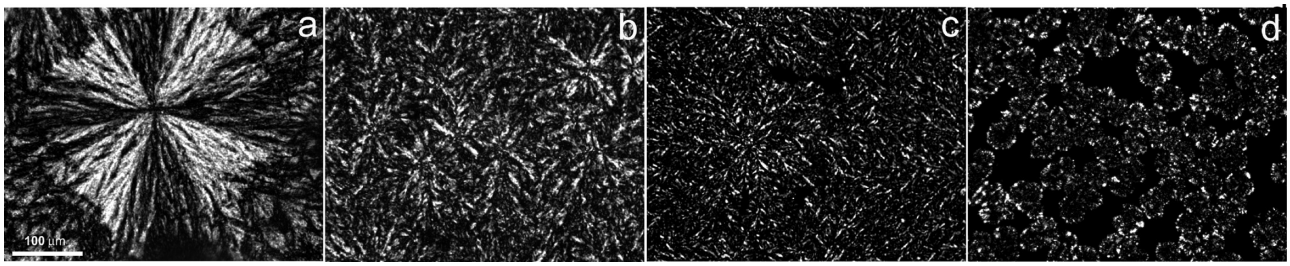

Figure 1. PLM micrographs of mixtures of fully hydrogenated canola oil (FHCO) and high oleic sunflower oil (HOSO) in the β polymorphic form. a, 100% FHCO; b, 70%FHCO; c, 50% FHCO; d, 30% FHCO.

suspended in cold isobutanol approximately in the ratio 1:50 using a glass stirring rod to obtain a uniform suspension. The fat plus isobutanol mixtures were homogenized at 30 000 rpm with a rotostator (Power Gen 125, Fisher Scientific) for 10 min. Then, the crystals were collected by vacuum filtration through a glass fiber filter of 1.0 μm pore size. After filtration, the recovered solid was resuspended in cold isobutanol and rehomogenized for 10 min using the rotostator in order to obtain a suitable dispersion of crystals. Finally, the mixtures were sonicated at 10 °C for 60 min using an ultrasonic processor (Bransonic 1210R-DTH, Branson Ultrasonic Corporation, Danburry, CT, USA) to complete the dispersion of the fat crystals. Assuming Couette type flow at the rotostator tip (radius = 3 mm, gap size = 200 μm), we estimated a tip shear rate of 47 000 s^{-1}. The Peclet number is the ratio between the shear rate and the rotational diffusivity of an object in that shear field, D_r, where $D_r = 3k_BT/\pi\eta d_p^3$. Assuming that in order to align the object in the shear field, a 10-fold larger shear rate relative to the rotational diffusivity is required, and for a spherical particle of diameter d_p = 100 nm, a shear rate of 112 000 s^{-1} would then be required (T = 283 K, isobutanol viscosity, η = 0.0033 Pa s, $k_B = 1.38 \times 10^{-23}$ J/K). Thus, the shear rate chosen is high enough to break low micrometer-scale objects, but not too high to disrupt nanometer-scale objects.

Five microliters of dispersion were placed on a copper grid with perforated carbon film (Canemco-Marivac, Quebec, Canada), and excess liquid was blotted automatically for 2 s using filter paper. A staining aqueous solution of 2% of uranyl acetate was used to enhance contrast. Subsequently, the sample was transferred to a cryo holder (Gatan Inc., Pleasanton, CA, USA) for direct observation at −176 °C in a FEI Tecnai G2 F20 energy-filtered Cryo-TEM operated at 200 kV in low dose mode. Energy filtering was used to improve image contrast by eliminating inelastically scattered electrons, which causes a blurring effect on micrographs. Zero-loss energy-filtered images were taken using a Gatan 4k CCD camera. Micrographs were stored and analyzed using DigitalMicrograph software (USA). Image J 1.42q software (USA) was employed for a semiautomatic analysis procedure.

Statistical Analysis. Data were processed using GraphPad Prism 5 software (GraphPad Software, Inc., San Diego, CA, USA). Values reported correspond to the means and standard errors of the determinations. A student t test was used to evaluate statistical significance in the observed changes in crystal dimensions. All statistical tests were two-tailed with a P-value < 0.05 taken to indicate statistical significance.

Results and Discussion

Many studies have demonstrated the importance of the microstructural level (crystal agglomerate size, shape, and spatial distribution) in defining macroscopic physical properties in fats. Changes in temperature, polymorphism, chemical composition, and solid fat content can all influence the microstructure of TAG crystal networks.[8−10,12,19,30−34] What still remains unknown, however, is the structure in the length scale of a few nanometers. The nanoscale in TAG crystal networks has not been characterized, and no systematic studies have been performed in this area. Furthermore, the relationship between the nano- and the microstructure and the effects on the physical properties of TAG crystal networks has never been considered before.

Figure 1 shows micrographs for blends of FHCO and HOSO with increasing quantities of HOSO, in the β polymorphic form, using polarized light microscopy (PLM). The predominant crystal morphologies observed in all samples are a central core of tightly packed needles surrounded by radially oriented needle-like crystals, that is, spherulites. These spherulites are consistent with the β polymorphic form as indicated previously by deMan.[35] Samples with 100% of FHCO (Figure 1a) presented a very densely packed microstructure characterized by the presence of big aggregates with well-defined Maltese cross patterns. Spherulite growth was limited by the presence of neighboring agglomerates.

The size of fat crystals at the microstructural level is strongly influenced by the supersaturation in the melt during crystallization and the cooling rate.[19,33,36−42] The degree of supersaturation ($\ln \beta$) in the blends was calculated as

$$\ln \beta = \frac{\Delta H_m}{RTT_m}(T_m - T) \quad (2)$$

where ΔH_m is the enthalpy of melting, T_m is the melting temperature, T is the crystallization temperature, and R is the gas constant. The purpose was to be able to correlate possible structural changes that may occur at any level in the crystalline network with modifications in the supersaturation values. The results are given in Table 1 along with the values of T_m, ΔH_m, and chemical potential difference ($\Delta\mu$) between the solid and the melt. $\Delta\mu$ represents the driving force for crystallization and is given by

$$\Delta\mu_{solution} = RT \ln \frac{c}{x} \quad (3)$$

$$\Delta\mu = \Delta H \frac{T_m - T}{T_m} \quad (4)$$

where c is the fraction soluble at supersaturated conditions, x is the fraction soluble at saturated conditions of the same component, c/x is the supersaturation ratio β.

The PLM micrographs show that the addition of sunflower oil does not influence directly the crystal morphology; however, a gradual reduction in spherulite size and a decrease in network density as a function of dilution is evident (Figure 1b−d). These results are in agreement with earlier reports employing similar fat blends.[41,43−45]

Historically, the term "fat crystal", as a constituent of a fat crystalline network, was attributed and accepted as those crystalline structures formed within the length scale of several micrometers. According to Hoerr,[46] crystals can have sizes ranging from 1 to 100 μm depending of the predominant polymorphic form. Moreover, numerous early publications reported crystal

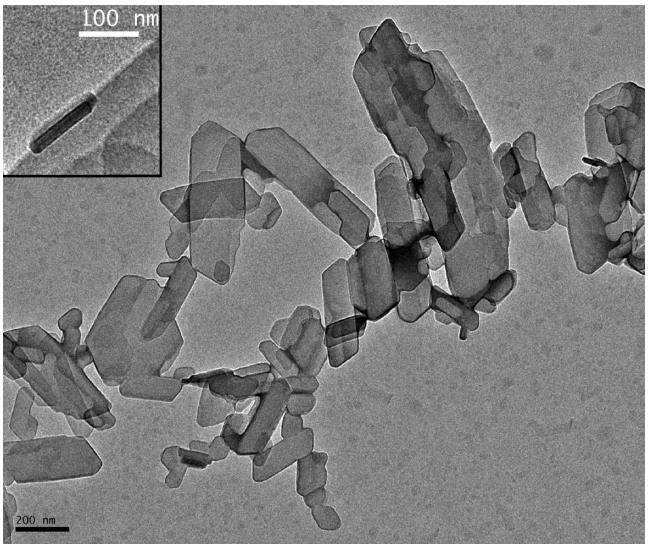

Figure 2. Extracted nanocrystals of tristearin (100% of FHCO; supersaturation value of 5.9) in the β polymorphic phase. The cryo-TEM technique gives rise to the individual structural elements in the fat sample after solvent treatment. Inset: nanoplatelet side view.

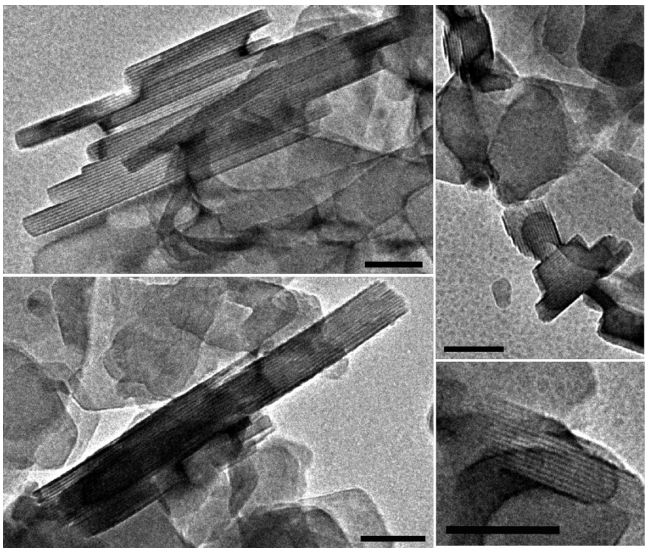

Figure 3. Cryo-TEM images showing the side view/thickness of the selected nanocrystals with a planar layered internal structure. The magnification bar corresponds to 100 nm.

sizes in the range of several micrometers.[8,10,16,47−50] In an early review by deMan and Beers,[8] a comment was made that crystal sizes range from 0.1 to 20 μm, whereas aggregates of crystals, spherulites, or flocs can reach sizes of over 100 μm.

The fact that many authors[8,10,16,47−50] have always considered the structural level in the micrometer range (defined as mesoscale) as the lowest stage in the fat crystalline network is, in part, a consequence that fat crystals do not behave as single units. On the contrary, crystals appear to grow due to the aggregation of smaller units, leading to the formation of larger structures. Additionally, electron microscopy techniques are difficult to perform on fats since they tend to melt, and the presence of oil in the samples interferes with nanoscale visualization. As a consequence, most of the research work was focused at the mesoscale, leaving a gap between structures in the length scale of a TAG lamella (~30−60 Å) and single TAG polycrystals (~1−3 μm), that is, the nanoscale.

In an attempt to remove the liquid oil present between fat crystals and release the nanostructural elements from the fat network, a sample treatment was developed in this work. It consists of the removal of all the liquid oil by a cold solvent and the mechanical disruption of the structural network in order to be able to image single nanocrystal units employing cryo-TEM. Cold solvent (10 °C) was chosen in order to maximize the recovery of solid fraction. Chawla and deMan[16] reported that solvent treatment allows the quantitative separation of the solid and liquid phases of fat.

To establish the solvent or solvent combination to be used, isobutanol, methanol and their mixtures were tested for their ability to dissolve high oleic sunflower oil while minimizing the dissolution of fully hydrogenated canola oil. After several studies, it was determined that isobutanol (since it has an intermediate polarity) better suited the requirements of this study, and was therefore chosen for further investigation. Figure 2 displays a small but representative part of the sample in the β-modification obtained by cryo-TEM after the solvent treatment. Fat crystals are clearly discernible individually from each other, as well as the platelet-like shape is revealed. Unruh et al.[22] and Bunjes et al.[23] reported a similar morphology working with crystallization of TAGs from aqueous emulsions of TAGs dissolved in an organic solvent.

Since the nanoplatelets were clearly distinguishable, we could not only determine their size accurately but also determine the angles of the platelets' corners. Image analysis yielded a value of 60° for the corner angles, in close agreement with crystallographic work,[51,52] where the crystallographic angle γ in the *ab* plane was reported to range from 57 to 62°.

On some occasions, crystals overlap which can be diminished by diluting the dispersion to be placed on the microscope grid. It is interesting to note that the nanoplatelet thickness can be measured from the side view of some particles (Figure 2, inset).

The platelet shape of the nanocrystals favors the particle orientation parallel to the plane of observation; therefore, we generally can visualize crystal lengths and widths. However, in some cases a side view was accessible. It is remarkable to us that we could observe a well-defined "layered" internal structure in these particles from this perspective (Figure 3). This appearance can be attributed to the molecular ordering and stacking of TAGs into layers or lamellae which later constitute the crystal thickness. These observations confirm that the molecular clusters which lead to the formation of a nanoplatelet during crystallization are not destroyed during sample preparation since shearing forces are not high enough for this to happen.

Measurements of the distance between each internal strip revealed values from 4 to 6 nm for all fat blends. Particularly, samples with 100% of FHCO, in the β polymorphic form (and supersaturation values of 5.9), revealed values of 4.23 $\pm$ 0.76 nm. This result was in agreement with determinations using small angle powder X-ray diffraction (SAXRD) which showed a small angle reflection at 4.5 nm. Our observations agree well with those reported by Bunjes et al.[23] who could also observe the internal structure of TAG crystals; however, it is worth noting that these authors worked on colloidal suspensions of TAG. Thus, although the constituents were similar, the fat matrix under study was not a native fat crystal network.

The treatment with isobutanol was relatively gentle on the crystalline phase in the fat crystal network, and allowed for the quantification of the size and shape of the nanoplatelets.

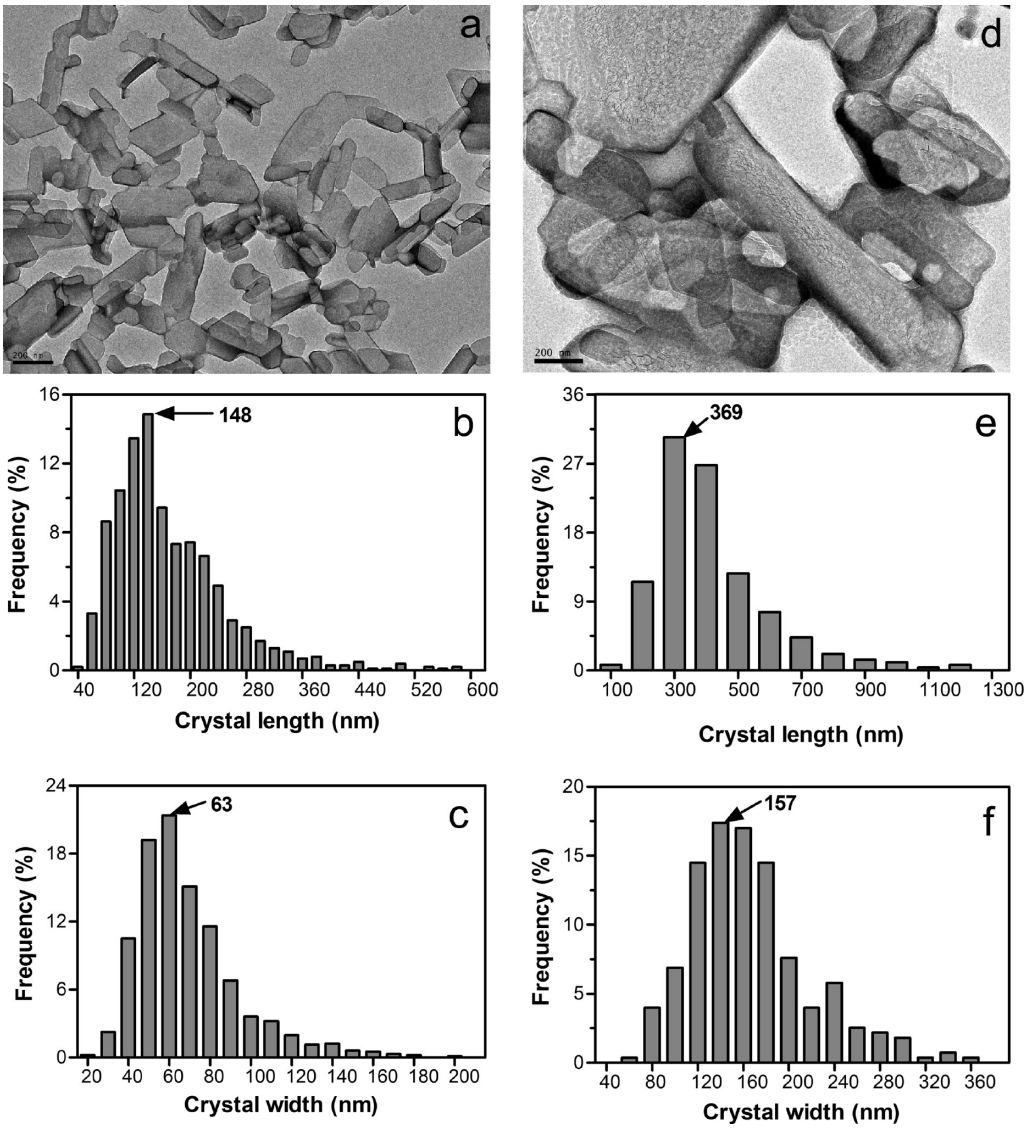

Figure 4. Cryo-TEM micrographs of blends with supersaturation values of 5.9 (100% of FHCO, a) and 4.8 (30% of FHCO, d) in the β polymorphic phase. Length and width frequency distributions for the blends with 100% (b, c) and 30% of hardstock (e, f), respectively. The corresponding arithmetical mean values are shown; the standard error (SE) is $\leq 1.5\%$ in all samples.

Imaging by cryo-TEM was performed at different stages of the solvent extraction and mechanical disruption treatment. Both for the early and intermediate stages of the procedure, we could visualize large pieces of irregularly shaped polycrystalline aggregates, which was evidence that the process of structural breakdown was not complete and a longer or more drastic treatment was required to release single nanocrystals. Not every extraction yielded suitable nanoplatelets. Subtle changes in temperature or mechanical agitation can lead to complete dissolution of the crystals. Edge rounding in the nanoplatelets is an indication of dissolution and can be used as a "quality control" parameter to judge extraction quality. The shelf life of the extracted crystals was 48 h at 5 °C. Chawla and deMan[16] also found isobutanol to be an appropriate oil extraction solvent in margarines and shortenings.

Figure 4 shows cryo-TEM micrographs of the blends with 100% (Figure 4a) and 30% (Figure 4d) of FHCO (supersaturation values of 5.9 and 4.4, respectively). It is possible to observe a variety of platelet sizes in both samples; nevertheless, it is clear that smaller crystals are present in blends with higher saturation values (100% of FHCO).

A semiautomatic image analysis procedure was employed to quantify the platelet dimensions. The resultant frequency distributions of particle lengths and widths confirm the visual examinations. In samples with 100% of FHCO the arithmetic mean sizes are 148 nm and 63 nm for length and width, respectively (Figure 4b,c). On the other hand, samples with 30% FHCO contain nanocrystals of considerably larger dimensions than those observed in blends with 100% FHCO. The mean length is 369 nm, while the mean width is 157 nm (Figure 4e,f). Therefore, the effect of the matrix dilution, and consequently lower supersaturation, is manifested as an increase in the size of the nanoplatelets without visible morphological changes.

Figure 5 shows an example of an X-ray pattern in the small and wide angle regions for the FHCO sample. In the wide angle region (or "short-spacing" region), the number and position of the peaks permit the identification of the different polymorphic forms of TAGs. In the small-angle region (or "long-spacing" region), the position of the peaks provides information on the size of the TAG chain length and the angle of tilt of the TAG chains relative to the normal. Additionally, besides

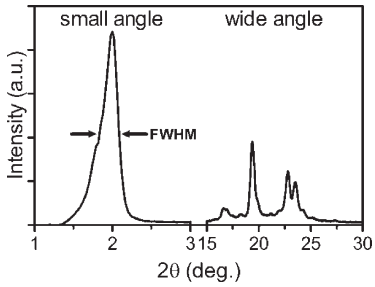

Figure 5. Example of a powder X-ray diffraction spectrum for fully hydrogenated canola oil (FHCO). In the small angle region, it is possible to observe the (001) reflection peak. The corresponding full wide at half-maximum (fwhm) is indicated with arrows. The peaks detected in the wide angle region determine the orthorhombic (β) polymorphic form present in the sample.

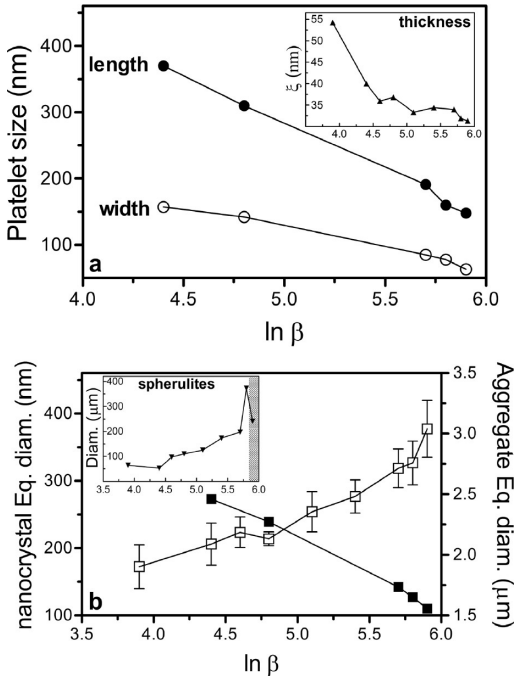

Figure 6. Platelet sizes as a function of supersaturation (a). (b) Nanocrystal (filled symbols) and aggregate equivalent diameters (open symbols) versus the supersaturation values. Inset: Spherulite size as a function of supersaturation values.

the reflection corresponding to the (001) plane, it is also possible to clearly observe higher order reflections. From the full width at half-maximum (fwhm) of the (001) reflection, it is possible to calculate the crystalline domain size (ξ), which represents the thickness of the platelets, using the Scherrer equation.[28] Peak broadening increases with the diffraction angle; therefore, it is important that this analysis is carried out only in the small angle region, preferably on the (001) reflection, and not higher order reflections.

Figure 6a shows the changes in nanocrystal dimensions as a function of changing supersaturation values (ln β). As it was discussed before, both platelet length and width diminish as the system's supersaturation increases. In addition, the nanocrystal thickness, obtained by the Scherrer analysis of the (001) X-ray reflection, displays the same tendency: nanocrystal thickness values decrease with an increase in the proportion of FHCO in the blend (Figure 6, inset). The results show that there is a reduction of approximately 40% in the platelet

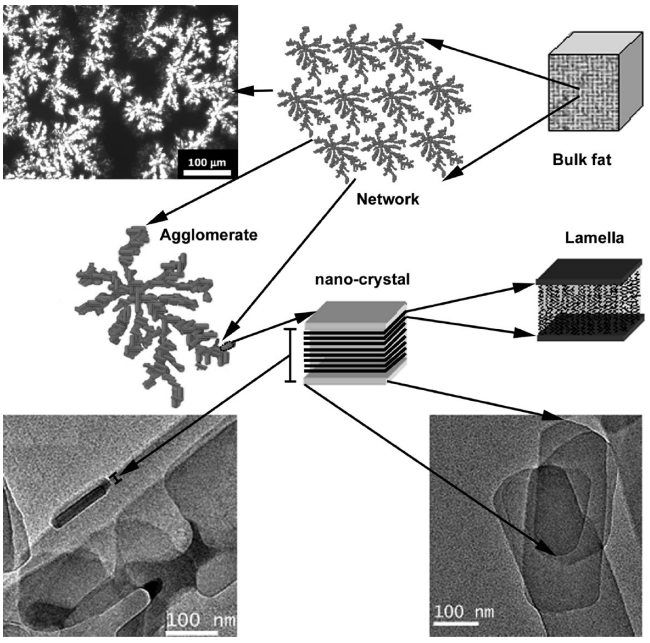

Figure 7. Schematic representation of the different levels of structure in a bulk fat. The platelet-like shape and thickness corresponding to the nanocrystal can be clearly observed on the cryo-TEM micrographs. The created TAG network can be appreciated through the PLM micrograph.

thickness when the system supersaturation changes from 3.9 to 5.9.

In our view, a very important finding in this work was the excellent agreement between the nanoplatelet thickness obtained by cryo-TEM and SAXRD. When applying the Scherrer's analysis to the SAXRD patterns in samples containing 100% of FHCO, the average domain size was 31.32 ± 0.07 nm. In addition, the platelet thickness measured from the cryo-TEM images was 31.2 nm, which is almost identical to the thickness value obtained by SAXRD.

In order to compare data obtained at the nanostructural level with those acquired from the microstructural analysis (by PLM), particle equivalent diameters at the nano- and microscale were calculated and plotted versus supersaturation (Figure 6b). Interestingly, equivalent diameters of microstructural elements (including aggregates and spherulites, Figure 6b and inset, respectively) display an opposite trend to the one observed for nanostructural particles as a function of supersaturation (Figure 6b). Aggregates behave in the same way as the spherulites; in fact we can consider aggregates as an early stage in the development of spherulitic-type structures. As the supersaturation increases, the median of the size distribution of aggregates and spherulites increases since more TAG components are available in the melt for crystalline growth under these conditions (Figure 6b and inset). The size of the aggregates determined by PLM ranged from 1.9 μm at a supersaturation value of 3.9 to 3.0 μm at a supersaturation of 5.9; this is an increase of approximately 1.6 times. Moreover, we observed that with an increase in the proportion of FHCO, the average length of the spherulite branches increases (Figure 6b, inset). At high supersaturations, the growth of highly branched fibers is favored and the successive branching at the growth front of the fibers develops a space-filling spherulitic network. At a supersaturation value of 5.9, it is possible to observe a decrease in the spherulitic sizes (indicated as a shaded part in the graph, Figure 6b, inset). This unexpected

result can be attributed to the interruption of the spherulites growth by direct contact with neighboring spherulites. Therefore, as it was pointed out before, supersaturation seems to affect the nanoscale and mesoscale in an opposite fashion. These results should tempt us to speculate further on the mechanism by which nanocrystals interact and aggregate into a three-dimensional network. It is currently unknown how nanoplatelet size affects spherulite growth and its structure. A great challenge remains to find the relationship between the nano- and the mesoscale. Recent work by Ueno et al.[53] using microbeam X-ray analysis of trilaurin spherulites may prove useful in the elucidation of how nanolevel packing of TAGs results in the characteristic mesoscale morphology of a spherulite.

Work in our laboratory over the years has focused on establishing relationships between the structure of fat crystal networks at different length scales and macroscopic functionality, particularly mechanical properties. Fat crystal networks display a complex structural hierarchy. This characterization of the nanoscale in fats allows us to present an updated scheme of the structure of these materials at different length scales (Figure 7). The primary crystal in TAG polycrystalline networks is a nanoplatelet. These nanoplatelets are the result of the stacking of several TAG lamellae. The internal structure of the nanoplatelets consists of stacked TAG bimolecular lamellae. Nanoplatelets flocculate to form larger aggregates which then pack with other aggregates in a closed pack fashion for a continuous three-dimensional network.

Conclusions

In this study, we characterized the nanoscale in TAG polycrystalline networks. The primary crystals of such a networks are nanoplatelets which were isolated using a cold isobutanol extraction technique and imaged using cryo-TEM. Nanoplatelet dimensions were extremely sensitive to the supersaturation conditions in the melt, with sizes decreasing as a function of increasing supersaturation. The internal structure of the nanoplatelets was characterized using small-angle X-ray diffraction and Scherrer analysis. Direct visualization of TAG molecular packing within the nanoplatelet was achieved and agreed quantitatively with domain size estimates from the Scherrer analysis. Future research will focus on the effects of external fields and chemical modification on nanoplatelet dimensions and morphology with the hopes of developing the first rational nanomanipulation in these materials for engineering macroscopic physical properties.

Acknowledgment. The authors thank The Natural Sciences and Engineering Research Council of Canada and Advanced Foods and Materials network for the financial support. The authors are grateful to Prof. Gianfranco Mazzanti for the many useful discussions on fat nanoscale structure.

References

(1) Marangoni, A. G. *Trends Food Sci. Technol.* **2002**, *13*, 37–47.
(2) Marangoni, A. G. In *Fat Crystal Networks*; Marangoni, A. G., Ed.; Marcel Dekker: New York, 2005; Chapter 12, pp 413−440.
(3) Tang, D.; Marangoni, A. G. *Adv. Colloid Interf. Sci.* **2006**, 128–130.
(4) Beckett, S. T. In *The Science of Chocolate*; The Royal Society of Chemistry: Cambridge, 2000; Chapter 6, pp 85−103.
(5) van den Tempel, M. *J. Colloid Sci.* **1961**, *16*, 284–296.
(6) Nederveen, C. J. *J. Colloid Sci.* **1963**, *18*, 276–291.
(7) van den Tempel, M. *J. Colloid Interface Sci.* **1979**, *71*, 18–20.
(8) deMan, J. M.; Beers, A. M. *J. Texture Stud.* **1987**, *18*, 303–318.
(9) Heertje, I.; Leunis, M.; van Zeyl, W. J. M.; Berends, E. *Food Microstruct.* **1987**, *6*, 1–8.
(10) Heertje, I. *Food Microstruct.* **1993**, *12*, 77–94.
(11) Vreeker, R.; Hoekstra, L. L.; den Boer, D. C.; Agterof, W. G. M. *Colloids Surf.* **1992**, *65*, 185–189.
(12) Marangoni, A. G.; Rousseau, D. *J. Am. Oil Chem. Soc.* **1996**, *73*, 991–994.
(13) Narine, S. S.; Marangoni, A. G. *Phys. Rev.* **1999**, *59*, 1908–1920.
(14) Narine, S. S.; Marangoni, A. G. *J. Cryst. Growth* **1999**, *198*, 1315–1319.
(15) Marangoni, A. G.; Rogers, M. *Appl. Phys. Lett.* **2003**, *82*, 3239–3241.
(16) Chawla, P.; deMan, J. M. *J. Am. Oil Chem. Soc.* **1990**, *67*, 329–332.
(17) Rousseau, D.; Hill, A. R.; Marangoni, A. G. *J. Am. Oil Chem. Soc.* **1996**, *73*, 973–981.
(18) Shi, Y.; Liang, B.; Hartel, R. W. *J. Am. Oil Chem. Soc.* **2005**, *82*, 399–408.
(19) Herrera, M. L.; Hartel, R. W. *J. Am. Oil Chem. Soc.* **2000**, *77*, 1197–1204.
(20) Marangoni, A. G.; Hartel, R. W. *Food Technol.* **1998**, *52*, 46–51.
(21) Litwinenko, J. W. In *Fat Crystal Networks*; Marangoni, A. G., Ed.; Marcel Dekker: New York, 2005; Chapter 16, pp 711−828.
(22) Unruh, T.; Westesen, K.; Bösecke, P.; Lindner, P.; Koch, M. H. J. *Langmuir* **2002**, *18*, 1796–1800.
(23) Bunjes, H.; Steiniger, F.; Richter, W. *Langmuir* **2007**, *23*, 4005–4011.
(24) Heertje, I.; Leunis, M. *Lebensm. − Wiss. U. Technol.* **1997**, *30*, 141–146.
(25) Weiss, R. G.; Terech, P. In *Molecular Gels Materials with Self-Assembled Fibrillar Networks*; Weiss, R. G.; Terech, P., Eds.; Springer: Dordrecht, Netherlands, 2006; pp 1−13.
(26) Jewel, G. G.; Meara, M. L. *J. Am. Oil Chem. Soc.* **1970**, *47*, 535–538.
(27) Poot, C.; Dijkshoorn, W.; Haighton, A. J.; Verburg, C. C. *J. Am. Oil Chem. Soc.* **1975**, *70*, 69–72.
(28) West, A. R. In *Solid State Chemistry and Its Applications*; West, A. R., Ed.; John Wiley & Sons: Chichester, West Sussex, England, 1984.
(29) Ahmadi, L.; Wright, A. J.; Marangoni, A. G. *Eur. J. Lipid Sci. Technol.* **2008**, *110*, 1014–1024.
(30) de Man, J. M. *Food Microstruct.* **1982**, *1*, 209–212.
(31) Heertje, I.; Eendenburg, V.; Cornelissen, J. M.; Juriaanse, A. C. *Food Microstruct.* **1988**, *7*, 189–193.
(32) Rousseau, D.; Forestiere, K.; Hill, A. R.; Marangoni, A. G. *J. Am. Oil Chem. Soc.* **1996**, *1* (73), 963–972.
(33) Martini, S.; Herrera, M. L.; Hartel, R. W. *J. Am. Oil Chem. Soc.* **2002**, *79*, 1055–1062.
(34) Awad, T. S.; Rogers, M. A.; Marangoni, A. G. *J. Phys. Chem. B.* **2004**, *108*, 171–179.
(35) deMan, J. M. *Proc. XV Int. Dairy Congr.* **1959**, *2*, 1010–1016.
(36) Litwinenko, J. W.; Rojas, A. M.; Gerschenson, L. N.; Marangoni, A. G. *J. Am. Oil Chem. Soc.* **2002**, *79*, 647–654.
(37) Herrera, M. L.; Hartel, R. W. *J. Am. Oil Chem. Soc.* **2000**, *77*, 1177–1187.
(38) Campos, R.; Narine, S.; Marangoni, A. G. *Food Res. Int.* **2002**, *35*, 971–981.
(39) Lopez, C.; Lesieur, P.; Bourgaux, C.; Ollivon, M. *J. Dairy Sci.* **2005**, *88*, 511–526.
(40) Pérez-Martínez, D.; Alvarez-Salas, C.; Charó-Alonso, M.; Dibildox-Alvarado, E.; Toro-Vazquez, J. F. *Food Res. Int.* **2007**, *40*, 47–62.
(41) Ahmadi, L.; Wright, A. J.; Marangoni, A. G. *Eur. J. Lipid Sci. Technol.* **2008**, *110*, 1025–1034.
(42) Ribeiro, A. P. B.; Grimaldi, R.; Gioielli, L. A.; Oliveira dos Santos, A.; Cardoso, L. P.; Goncalves, L. A. G. *Food Biophys.* **2009**, *4*, 106–118.
(43) Rousseau, D.; Forestière, K.; Hill, A. R.; Marangoni, A. G. *J Am Oil Chem. Soc.* **1996**, *2* (75), 1833–1839.
(44) Rousseau, D.; Marangoni, A. G.; Jeffrey, K. R. *J Am Oil Chem. Soc.* **1998**, *2* (75), 1833–1839.
(45) Rodriguez, A.; Castro, E.; Salinas, M. C.; Lopez, R.; Miranda, M. *J. Am. Oil Chem. Soc.* **2001**, *78*, 431–436.
(46) Hoerr, C. W. *J. Am. Oil Chem. Soc.* **1960**, *37*, 539–544.
(47) Manning, D. M.; Dimick, P. S. *Food Microstruct.* **1985**, *4*, 249–265.
(48) Juriaanse, A. C.; Heertje, I. *Food Microstruct.* **1988**, *7*, 181–188.
(49) Herrera, M. L.; Falabella, C.; Melgarejo, M.; Añon, M. C. *J. Am. Oil Chem. Soc.* **1999**, *76*, 1–6.
(50) Fitzgerald, A. M.; Barnes, O. J.; Smart, I.; Wilson, D. I. *J. Am. Oil Chem. Soc.* **2001**, *78*, 1013–1020.
(51) Skoda, W.; Hoekstra, L. L.; van Soest, T. C.; Bennema, P.; van den Tempel, M. *Kolloid Z. Z. Polym.* **1967**, *219*, 149–156.
(52) Van Langevelde, A. J.; Peschar, R.; Schenk, H. *Chem. Mater.* **2001**, *13*, 1089–1094.
(53) Ueno, S.; Nishida, T.; Sato, K. *Cryst. Growth Des.* **2008**, *8*, 751–754.